Interpreting STM images of the MnCu/Cu(100) surface alloy

D. Wortmann
Institut für Festkörperforschung, Forschungszentrum Jülich, D–52425 Jülich, Germany

S. Heinze
Institut für Festkörperforschung, Forschungszengtrum Jülich, D–524525 Jülich, Germany
and Zentrum für Mikrostrukturforschung, Universität Hamburg, D–20355 Hamburg, Germany

G. Bihlmayer and S. Blügel
Institut für Festkörperforschung, Forschungszentrum Jülich, D-52425 Jülich, Germany
(Received 19 January 2000)

$c(2\times2)$MnCu/Cu(100) is an ordered two-dimensional surface alloy that exhibits a checkerboard arrangement of Mn and Cu atoms on the Cu(100) surface. Mn buckles outwards by 0.3 Å with respect to Cu and in all previous scanning tunneling microscopy (STM) experiments only one chemical species was imaged which was assumed to be Mn. We analyze the STM results by first-principles calculations based on the density-functional theory and show that Cu rather than Mn is imaged, while indeed Mn is imaged as single Mn impurities at Cu(100). We explain this result in terms of the formation of Mn states bridging over the Cu atoms. These Mn states are characteristic for Mn in a $c(2\times2)$MnCu surface alloy. Missing Mn atoms break this bridging bond and the surrounding Cu atoms are imaged as depressions.

I. INTRODUCTION

In the past few years, the $c(2\times2)$MnCu/Cu(100) developed to a model system for a magnetic, two-dimensional, ordered surface alloy. The growth[1–4] and the structural, electronic, and magnetic properties of this system were investigated by quantitative I/V low-energy electron diffraction[5] (LEED), photoemission,[6,7] and inverse photoemission[6] (BIS), soft-x-ray absorption (SXA) and emission[8–10] (SXE), and magnetic circular dicroism[11] (CMXD). From this we can conclude that $c(2\times2)$MnCu/Cu(100) is structurally well-defined and stable over a large temperature range, with a large magnetic moment for Mn. It is a substitutional surface alloy that forms a checkerboard type arrangement of Mn and Cu atoms of one monolayer (ML) thickness. The atomic structure is characterized by a considerable atomic corrugation (Mn buckles outward by 16.6% of the Cu interlayer distance, which corresponds to 0.3 Å) in the ordered surface alloy layer. Interesting enough, no ordered bulk alloy exists for the Cu-Mn system. Early total energy calculations have shown that the corrugation[12] of the $c(2\times2)$MnCu/Cu(100) surface alloy layer is due to the formation of a large magnetic moment of the Mn atoms. Meanwhile, a significant number of additional $c(2\times2)$ MnX/X surface alloys have been found, i.e., $X=$Cu(110),[13] Co(100),[14] Ni(100),[15] Pd(100),[16] and Ag(100).[17–19]

A recent set of scanning tunneling microscopy (STM) studies[20–22] confirmed the existence of a $c(2\times2)$ surface unit cell, although only *one* chemical component of the surface alloy was imaged (for a typical STM image, see Fig. 5). Due to the large outwards buckling of the Mn atoms with respect to the Cu surface atoms it was anticipated that (i) the Mn atoms should be imaged as protrusions and the Cu atoms as depressions, and (ii) it should be possible to determine the outward buckling of Mn by the STM. This interpretation is in accordance with the conventional understanding of STM images of metal surfaces, which is based on the concept that electrons screen the positive charge of the nuclei, and the STM tip follows the density distribution of the surface atoms. It was confirmed by an STM experiment[22] that a single Mn impurity in the Cu(100) surface is indeed imaged as a protrusion. Although the above-noted experimental findings lead to a consistent structural model of an ordered MnCu surface alloy, the estimated outward buckling of Mn varies significantly among the experiments.[20–22]

In this paper we analyze the STM images of the $c(2\times2)$ MnCu/Cu(100) surface alloy on the basis of the model of Tersoff and Hamann[23] and first-principles electronic structure calculations. We show, while indeed a single Mn impurity is imaged as a protrusion, for a $c(2\times2)$ MnCu/Cu(100) surface alloy the Cu atoms and not the Mn atoms are imaged. We show that the chemical identification cannot be derived from atomic arrangement but is rather determined by the electronic structure. We explain this result in terms of the formation of surface bonds between next-nearest-neighbor Mn atoms bridging over the Cu atoms. This explains also images of Mn antisite defects (Cu surface atoms that have not been substituted by Mn atoms during the growth process) as depressions since missing Mn atoms break this bridging bond and the surrounding Cu atoms are imaged as depressions. Since the image is determined by details of the electronic structure, a determination of the relaxation based on STM is bound to fail. The paper is organized as follows: Section II outlines briefly the computational method and computational details. Section III summarizes the theoretical determination of the STM images. In Sec. IV we present our results. We focus first on the STM simulation of a perfect $c(2\times2)$ MnCu surface alloy and comment on changes of the simulated images due a possible $p(2\times2)$ antiferromagnetic order or due to a possible underestimation of the exchange

splitting. Then, we investigate the STM image of a $p(2\times2)$ MnCu surface alloy as a model of a single Mn impurity and finally we compare our result with an existing STM image and focus on the explanation of defects. In the last section, we draw some conclusions of this work.

II. COMPUTATIONAL DETAILS

We performed *ab initio* calculations using density-functional theory as implemented in the FLEUR code. This program implements the full-potential linearized augmented plane-wave (FLAPW) method[24,25] in film geometry. In all calculations we used the local spin-density approximation in the parametrization of Volko, Wilk, and Nusair.[26]

Four different configurations were investigated: the $c(2\times2)$ MnCu surface alloy with all atoms at ideal lattice positions and the $c(2\times2)$ MnCu surface with the surface atoms at the positions determined by Wuttig *et al.*[5] performing I/V LEED experiments. To simulate a single Mn impurity substituting a Cu atom we calculated the $p(2\times2)$ MnCu surface alloy with one Mn atom per three Cu surface atoms. This system was also calculated with the atoms on ideal crystal positions and with the Mn atom displaced outwards by 0.3 Å assuming that the relaxation of Mn in a $c(2\times2)$ and in a $p(2\times2)$ alloy is very similar. In all cases the experimental lattice constant was used ($a_0=6.83$ a.u.).

The $c(2\times2)$ surface alloy was simulated by an 11-layer film with semi-infinite vacuum on both sides. Self-consistency was obtained using 36 special $\mathbf{k}_\parallel$ points[27] in the irreducible wedge of the two-dimensional (2D) Brillouin zone (BZ). After reaching self-consistency the local density of states (LDOS) in the vacuum was calculated using 91 $\mathbf{k}_\parallel$ points.

The surfaces with a $p(2\times2)$ unit cell were simulated using a nine-layer film. This thickness is sufficient to keep the interactions between the two surfaces so small that the calculated STM images are not effected. The self-consistency was reached with 36 $\mathbf{k}_\parallel$ points and the LDOS was obtained with 78 $\mathbf{k}_\parallel$ points.

To check whether an underestimation of the magnetic moment caused by the exchange correlation approximation is crucial for our results we performed one calculation in which the splitting of the minority and majority band of the Mn d states was enhanced by introducing an additional Hubbard-like exchange constant $U=1.5$ eV as an additional parameter. This shifted the Mn d band by approximately 1.5 eV while our main results remained unaffected.

III. THEORETICAL DETAILS OF THE STM ANALYSIS

We calculated the STM current according to the model of Tersoff and Hamann.[23] This model was originally derived using an s-wave tip. It has successfully been applied to metal surfaces[30,32,31,29] in the past and according to an analysis by Tersoff[28] this simple model should hold true for metal surfaces with more general tips. In this model the tunnel current is proportional to the LDOS of the sample at the location of the outermost tip atom and thus it is given by

$$I(\mathbf{r}_\parallel,z,U)\propto\int_{-\infty}^{+\infty} g_{U,T}(\epsilon)\, n(\mathbf{r}_\parallel,z,\epsilon_F+\epsilon)\, d\epsilon, \tag{1}$$

where ϵ_F is the Fermi energy, $n(\mathbf{r}_\parallel,z,\epsilon_F+\epsilon)$ is the LDOS of the sample evaluated at the lateral ($\mathbf{r}_\parallel$) and vertical (z) position[33] of the tip. $g_{U,T}(\epsilon)$ denotes the difference of the Fermi function f_T at $\epsilon_F-eU+\epsilon$ and $\epsilon_F+\epsilon$, where U is the applied bias voltage.

The corrugation amplitude Δz, i.e., the maximum variation in the vertical position of the tip as it scans the surface at constant current, has been calculated as described in Ref. 30:

$$\Delta z(z,U)\propto\frac{\int g_{U,T}(\epsilon)\,[n_2(z,\epsilon)\Delta\Phi_2+n_3(z,\epsilon)\Delta\Phi_3]\,d\epsilon}{\int g_{U,T}(\epsilon)\,(\partial/\partial z)n_1(z,\epsilon)\,d\epsilon}, \tag{2}$$

where $n_{1,2,3}$ are the lowest-order LDOS star coefficients. These star coefficients are obtained expanding the LDOS in symmetrized 2D plane waves (''star'' functions Φ_s) with z-dependent coefficients:

$$n(\mathbf{r}_\parallel,z,\epsilon)=\sum_s n_s(z,\epsilon)\,\Phi_s(\mathbf{r}_\parallel). \tag{3}$$

$\Delta\Phi_{2,3}$ used in Eq. (2) denotes the difference of the values of the corresponding star functions between the position of maximal and minimal current within the surface unit cell.

As we present calculations on a $c(2\times2)$ superstructure on a fcc(100) surface we will briefly describe the first three star functions of a square lattice. The first star function, $\Phi_1(\mathbf{r}_\parallel)=\Phi_1$, is simply a constant independent of $\mathbf{r}_\parallel$ and does not contribute to the corrugation pattern. Its coefficient n_1 must be positive since it represents the charge integrated over the 2D unit cell. The second star function, $\Phi_2(\mathbf{r}_\parallel)$, has a maximum at the corners of the $c(2\times2)$ surface unit cell and a minimum in the center. In all our calculations the Mn atoms are placed at the corners of the surface unit cell. We use the sign convention that a negative second star coefficient will lead to a negative contribution to the corrugation amplitude $\Delta z_2=\mathrm{sgn}(n_2)|n_2/n_1|$. This corresponds to an STM image that shows the Mn atoms as depressions and the Cu atoms as protrusions. A positive corrugation amplitude means protrusions at Mn positions and depressions at Cu positions. The third star function, $\Phi_3(\mathbf{r}_\parallel)$, has a maximum at all atom positions and a minimum at all hollow sites. This star does not distinguish between Mn and Cu atoms, and thus the coefficient n_3 determines the amount of the $p(1\times1)$ surface cell seen in the STM image. In corrugation amplitude plots showing this third star contribution only, a negative corrugation amplitude refers to an STM image showing the hollow sites as protrusions and the atom sites as depressions, while a positive corrugation amplitude refers to a ''normal'' image with depressions at the hollow sites and protrusions at the atom sites.

In the calculations the star coefficients with order higher than three were neglectably small. Therefore, we calculated the total corrugation amplitude by the first three stars only. In the plots of the total corrugation amplitude the sign convention of the second star coefficient was used, $\Delta z_{tot}=\mathrm{sgn}(n_2)|\Delta z_{tot}|$.

From a simple WKB-like derivation[30] it can be deduced that the different star contributions to the LDOS decay differently into the vacuum depending on the $\mathbf{k}_\parallel$ points in the 2D Brillouin zone:

$$n_s(\mathbf{k}_\parallel, z) \propto \exp[-z\sqrt{2m|\epsilon|/\hbar^2 + (\mathbf{k}_\parallel + \mathbf{G}_\parallel^s)^2}] \times \exp(-z\sqrt{2m|\epsilon|/\hbar^2 + \mathbf{k}_\parallel^2}), \quad (4)$$

where $\mathbf{G}_\parallel^s$ is the wave vector of the plane waves forming the sth star function. For a square lattice, states at the high-symmetry points $\bar{\Gamma}$, $\bar{X}$, and $\bar{M}$ of the 2D Brillouin zone dominate the first, second, and third star contributions, respectively, at a large distance z from the surface.

At this point we would like to comment on the quantitive value of the corrugation amplitude. In reality, the corrugation amplitude depends on many factors, i.e., on the distance between tip and sample and also on the actual tip material and tip geometry. According to the model of Chen[34] the corrugation amplitude will increase with a more d_{z^2}-like tip. Since the exact atomic configuration of the tip and thus also the electronic configuration of the tip is unknown, it may not be modeled very well in the Tersoff-Hamann model. However, the calculated corrugation amplitude can be related to the experimental values by a factor that depends on the experimental details. Qualitative features such as the sign of the corrugation amplitude and the relative strength of the second and third star contributions, however, are well reproduced.

IV. RESULTS

A. The $c(2\times2)$ MnCu/Cu(100) surface alloy

We used two configurations to calculate STM images of the ordered $c(2\times2)$ MnCu/Cu(100) surface alloy. First, we studied the unrelaxed alloy with all atoms placed at the ideal Cu lattice sites. This system should allow the identification of effects due to the electronic structure of the system. To investigate the effect of the lattice relaxation on the STM image we used a second configuration with the Mn and the Cu atoms of the surface layer located according to the relaxation determined by Wuttig *et al.*[5] Surprisingly, despite the huge relaxation of Mn, many results do not depend significantly on the amount of surface relaxation, as a direct comparison between the two systems reveals.

The calculated corrugation amplitude of the STM image of the unrelaxed surface alloy, shown in Fig. 1, displays several interesting features. First, it can be seen that the second star coefficient dominates the total corrugation amplitude. This agrees with the experiments showing a distinct $c(2\times2)$ pattern with protrusions at one atom type and depressions at the other. Second, the total corrugation amplitude is negative for $U<1$ V. Keeping in mind our sign convention for the corrugation plots one deduces from Fig. 1 that the protrusions will be at the Cu positions of the surface at small bias voltages $|U|<0.5$ V as typically used in the experiments, i.e., $U\sim150$ mV in Ref. 21. Furthermore, this strong dominance of the $c(2\times2)$ pattern to the STM image is due to the minority spin contribution to the LDOS as one can see from the spin resolved graphs in Fig. 1. The dominance of the minority spin might be expected due to the fact that the majority Mn d bands are located approximately 1.5 eV below the Fermi energy. However, it must be noticed that the minority spin is not only responsible for the total corrugation amplitude, but also determines the Cu positions as protrusions. To find the most important states responsible for these protrusions we investigated the electronic structure in detail.

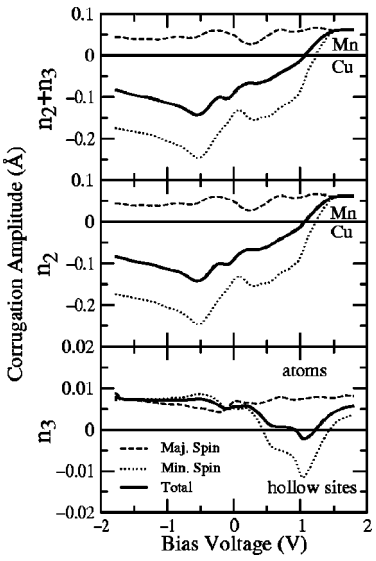

FIG. 1. Calculated corrugation amplitude for the $c(2\times2)$ MnCu surface alloy with all surface atoms at ideal Cu positions for a tip-sample distance of 4.7 Å. The upper panel shows the total corrugation amplitude as calculated from the second and third star coefficients, the middle panel shows the corrugation amplitude resulting from only second star contribution only, and the lower panel shows the corrugation amplitude resulting from the third star contribution only. In all plots, contributions from both spins individually and the resulting total spin unresolved corrugation amplitudes are shown. For n_2 and $n_2+n_3>0$ (<0) Mn (Cu) atoms are imaged. For $n_3>0$ (<0) atoms (hollow) sites are imaged.

Figure 2 shows both a bandstructure along the high-symmetry lines between the $\bar{X}$ and the $\bar{M}$ point and a plot of the second star coefficient of the LDOS integrated over all $\mathbf{k}_\parallel$ points of the 2D BZ. According to Eq. (4), states at the $\bar{X}$ point of the 2D BZ contribute most to the second star coefficient. One can identify several flat bands stretching from the $\bar{X}$ to the $\bar{M}$ point in the bandstructure which correspond to peaks in the star coefficient n_2. Most obviously, the flat minority bands just below the Fermi energy and at -0.4 eV, which are largely d electrons localized at the Mn surface atoms, are the main origin of the negative peaks in the LDOS. On the other hand the unoccupied Mn located states above 1 eV correspond to positive peaks in n_2.

Figure 3 shows the charge density distribution due to the minority state at -0.09 eV at the $\bar{X}$ point. This state, being predominantly localized at the Mn site, also spills out into the vacuum and stretches above the positions of Cu atoms to the next Mn atom. Since the STM current is proportional to the LDOS of the sample at the position of the tip, the STM will show the Cu atoms as protrusions even though the states which dominate the LDOS are mainly localized at Mn positions. At this point we would like to emphasize already that the formation of these states is characteristic for the Mn in the $c(2\times2)$ MnCu surface alloy only. In a $p(2\times2)$ MnCu

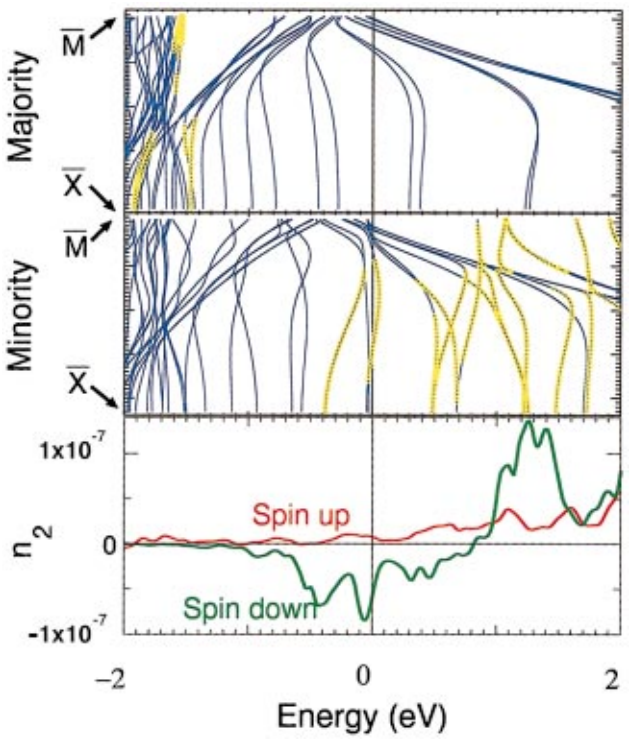

FIG. 2. (Color) Calculated band structure of the $c(2\times2)$ MnCu/Cu(100) surface alloy. The upper two panels show the majority and minority bands along the high-symmetry line from $\bar{X}$ to $\bar{M}$. *d*-like states, localized to more than 40% in the Mn muffin-tin spheres, are marked by yellow dots. The lower panel of the plot shows the second star coefficient to the LDOS as a function of the energy split into majority spin (red) and minority spin (green) contribution.

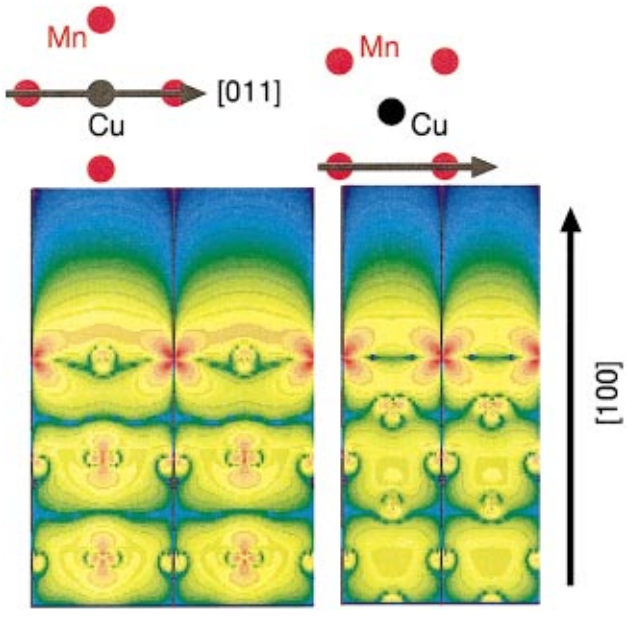

FIG. 3. (Color) Charge density plot of one single minority state just below the Fermi energy at the $\bar{X}$ point. Two different slices through two unit cells are shown. One is in the (011) plane showing the diagonal of the surface unit cell with both the Mn and the Cu atom, and the other is in the (010) plane showing only the Mn surface atoms.

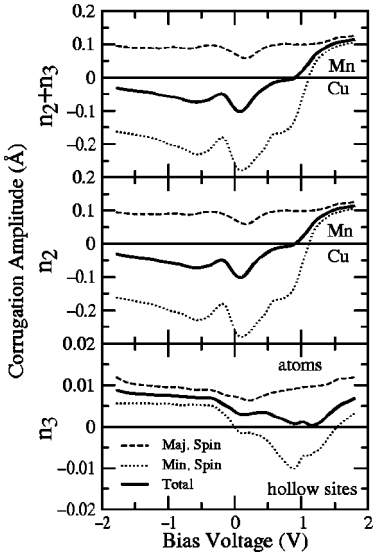

FIG. 4. Calculated corrugation amplitude for the relaxed $c(2\times2)$ MnCu surface alloy. Compared to Fig. 1, this figure shows a shift in the second star coefficient. For a detailed description of the figure see the Fig. 1 caption.

surface alloy with half the concentration of Mn atoms, these states are absent, i.e., the formation of these states depends on the nearest-neighbor Mn-Mn interaction in the $c(2\times2)$ MnCu alloy.

All results discussed so far are obtained using an unrelaxed surface. Since the measured buckling of the alloy is fairly large showing an outwards relaxation of Mn by 0.3 Å, STM is expected to image the Mn rather than the Cu positions. To investigate the influence of the relaxation we

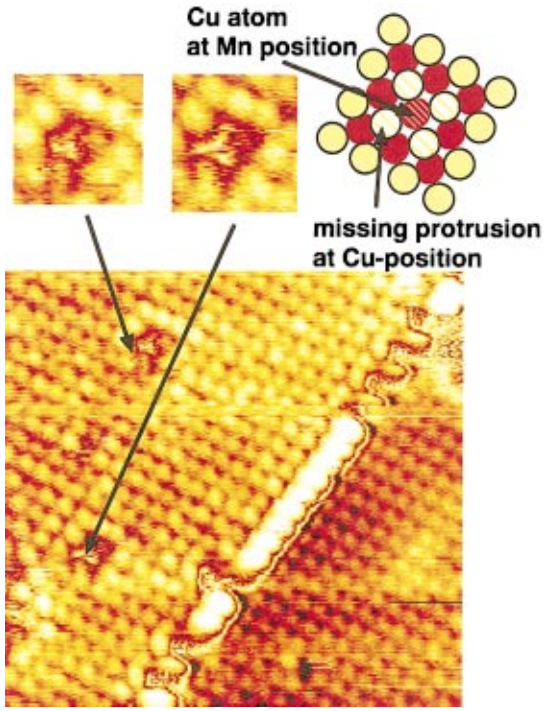

FIG. 5. (Color) STM image of the $c(2\times2)$ MnCu alloy. The $c(2\times2)$ unit cell is clearly visible on both sides of the step edge. Please note the two defects of four missing bright spots (figure from Ref. 21).

performed STM calculations on the relaxed $c(2\times2)$ alloy. Commonly, it was expected that the STM image will show a $c(2\times2)$ structure with protrusions at Mn atoms due to the relaxation. In our analysis this corresponds to a positive second star contribution to the corrugation amplitude. As shown in Fig. 4, the contribution of the second star coefficient and also the total corrugation amplitude is indeed shifted, but only by approximately $+0.05$ Å. Even more important, the corrugation amplitude does not change sign. Obviously, the surface relaxation reduces the contribution of the electronic effects to the STM image, but it is not the dominating factor. In particular, we show that the contribution of the electronic structure to the corrugation amplitude and the structural relaxation are not additive.

Until now, all investigations have been carried out under the assumption that the magnetic moments of the Mn atoms couple in parallel form and that the MnCu surface alloy is ferromagnetically ordered. This is consistent with total energy calculations of Rader *et al.*,[6] who found the ferromagnetic state to be the equilibrium state. Until now, this could not be confirmed experimentally. At present the Curie temperature is unknown. This motivated us to simulate an STM image and to calculate the corrugation amplitude of the $c(2\times2)$ MnCu/Cu(100) surface alloy with a possible $p(2\times2)$ antiferromagnetic superstructure. This magnetic superstructure exhibits a checkerboard arrangement of up and down spins within the Mn sublattice. Thus nearest-neighbor Mn atoms couple antiferromagnetically. Under conventional circumstances the STM tip is nonmagnetic and a magnetic contrast cannot be achieved. Consequently, the magnetically inequivalent Mn atoms are indistinguishable by conventional STM. Nevertheless, the electronic structure changes due to the antiferromagnetism. Our calculations show that irrespective of the magnetic state at experimentally relevant bias voltages of $|U|<0.5$ V we expect a $c(2\times2)$ pattern in which Cu will be imaged as protrusions. Only for fairly large bias voltages could differences in the corrugation amplitude between the ferromagnetic and the antiferromagnetic order be found. From this we can safely conclude that the actual magnetic structure will not inflict with the interpretation given above.

There are several indications that the calculations applying the local density approximation or the generalized gradient approximation[35] underestimate the magnetic moment of Mn in the MnCu surface alloy. One important experiment in this context was carried out by Rader *et al.*,[6] who determined the exchange splitting of Mn by photoemmission combined with inverse photoemmission to 5.5 eV, while we determined the theoretical exchange splitting to 2.5 eV. This raises the question whether the calculated STM image is an artifact of the underlying theoretical approximations. In order to check this, in the spirit of LDA+U calculations,[36] we increased artificially the exchange splitting by adding an additional constant potential term $U=1.5$ eV to the Hamiltonian, which is only applied to the Mn d electrons, and recalculated the corrugation amplitude. The additional potential term U moves the Mn majority states down to about 5 eV below the Fermi energy and the minority states upwards to about 2 eV above the Fermi energy. Despite these large changes of the local density of states, the minority density of states in the vicinity of the Fermi energy remains quite unaffected. The sign and the strength of the calculated corrugation amplitude do not alter significantly. From this we can conclude that the underestimation of the exchange splitting does not change our conclusion that Cu and not Mn is imaged by the STM.

The strong dependence of the STM image on the electronic contribution might give an indication why different experimental groups found very different results for the corrugation amplitude measured by STM. Presumably, not the surface relaxation was directly observed, but the electronic contribution to the corrugation amplitude or LDOS, respectively, was the origin of the experimental results. The assumption that the corrugation amplitude measured in an STM experiment can be related to the surface relaxation, as it is underlying in the work of Noh *et al.*,[20] van der Kraan and van Kempen,[21] and Wuttig *et al.*,[22] is unjustified from our point of view. Therefore, it is most likely impossible to deduce the surface buckling from these STM-based experiments.

B. $p(2\times2)$ MnCu alloys on the Cu(100) surface

In the paper of Wuttig *et al.*[22] a single Mn atom substituting a Cu atom in the Cu(100) surface was used to measure the buckling of a Mn atom by STM. Assuming that the buckling of a single Mn impurity and that of Mn atoms in the $c(2\times2)$ surface alloy is approximately the same, the STM experiment would give a direct estimate of the buckling of Mn in the alloy. We modeled the Mn impurity using a $p(2\times2)$ surface unit cell with one Mn and three Cu atoms in the surface layer in which, opposite to the $c(2\times2)$ surface alloy, no Mn atoms occupy next-nearest-neighbor sites. It turned out that this increase of the Mn-Mn distance is sufficient to destroy the state discussed in the $c(2\times2)$ alloy that bridges over the Cu atoms and extends into the vacuum.

The calculated corrugation amplitude of the unrelaxed $p(2\times2)$ MnCu alloy, not displayed here, shows virtually no chemical contrast between the Mn and the Cu atoms. The star coefficient n_2, which distinguishes between Mn and Cu, is small and the STM image is determined by the higher star coefficients. Consequently, the calculated STM image shows a $p(1\times1)$ surface pattern in which the atoms are imaged as protrusions. This clearly indicates that the states bridging over the Cu surface atoms, formed in the case of the $c(2\times2)$ surface alloys, are absent. Thus, one may expect that in the case of a single Mn impurity or in the case of the relaxed $p(2\times2)$ alloy, respectively, the corrugation measured by STM is directly related to the atomic arrangement. This is confirmed by a calculation, in which the Mn atoms were displaced outwards by 0.3 Å. In this relaxed configuration a strong chemical contrast is observed. Unlike the results for the $c(2\times2)$ MnCu alloy, in this case the Mn atoms are shown as protrusions. Concluding, one can deduce that the corrugation measured by STM for a $p(2\times2)$ surface alloy and probably also for a single impurity will be predominately determined by the atomic arrangement. Hence, Wuttig *et al.* have chosen a suitable approach to determine the surface relaxation of a single Mn impurity by STM.

The magnetic moment of a Mn atom in the relaxed $c(2\times2)$ MnCu/Cu(100) surface alloy and in a relaxed $p(2\times2)$ MnCu/Cu(100) surface alloy amounts to $3.85\mu_B$

and $4.05\mu_B$, respectively. This shows that the magnetic moment in the different configurations is nearly the same. As it has been shown in Ref. 37, the amount of Mn buckling depends basically on the size of the magnetic moment. Since the size of the magnetic moments of the two configurations are nearly unchanged, we expect a very similar buckling of a Mn atom as a single impurity. In retrospect, this confirms our assumption made on the relaxation of Mn in a $p(2\times2)$ MnCu surface alloy and this substantiates the assumption of Wuttig *et al.*[22] Together with the above finding, that for a single Mn impurity, the corrugation measured by STM is predominantly determined by the atomic structure and not by the the electronic structure, the approach of Wuttig *et al.* measuring the buckling of a single Mn atom provides a good estimate of the buckling of Mn in a surface alloy.

C. Comparison to STM experiments

An experimental finding substantiating our interpretation that the Cu atoms rather than the Mn atoms of a $c(2\times2)$ MnCu/Cu(100) surface alloy are imaged can be found in Fig. 5. The STM image shows a Cu(100) surface covered by about half a monolayer of Mn. A step edge separates two terraces. On both terraces a square pattern of bright spots is clearly visible. From the size of this pattern, which is two times larger than the surface unit cell of Cu(100), one can deduce, that it corresponds to the $c(2\times2)$ unit cell and not to the $p(1\times1)$ unit cell. Obviously, a high chemical contrast is observed. Only one type of atom is visible as a protrusion, while atoms of the other type are located at the dark spots of the square pattern. So far, this corresponds perfectly to the results presented here. Of course, the question whether the Cu or the Mn atoms are imaged cannot be answered from these observations.

At this point special attention should be given to the two defects on the left terrace. These defects consist of four missing bright spots of the $c(2\times2)$ pattern and they are observed to move with time. In the following, we interpret these defects as being due to one missing Mn atom in the surface alloy. An antisite defect, a Mn atom that failed to substitute a Cu atom during the growth process, would be one possible example of such a missing Mn atom. If one of the Mn atoms of the alloy is replaced by a Cu atom, the results obtained from the $p(2\times2)$ MnCu alloy suggest that the bonds bridging over the Cu atoms are broken and that the enhanced density of states in the vacuum above the Cu sites disappears. This looks then like a defect of four missing bright spots as observed in the STM image. The alternative interpretation would assume that the defects are formed by four missing Mn atoms. Since the defects of four bright spots are observed to move, the latter interpretation seems very unlikely. Therefore, the image of the defects give a clear indication in favor of the interpretation given here.

V. CONCLUSIONS

We have shown that the interpretation of atomically resolved STM images of multicomponent metal surfaces on the basis of the atomic arrangements are unreliable and misleading. In the case of the $c(2\times2)$ MnCu/Cu(100) surface alloy, according to our analysis, this interpretation is wrong. Even though the Mn atoms in this alloy stick out of the surface by 0.3 Å and all STM experiments have been interpreted, in the same manner, namely to image the Mn atoms as protrusions, we found the electronic structure to be more important than the atomic buckling for interpretation of the STM images. We think that for this particular example of a MnCu surface alloy, Cu is imaged as a protrusion and Mn as a depression. For single Mn impurities, Mn is imaged as a protrusion, in agreement with experiments. Our results are supported by STM images of defects, which are consistently explained as antisite defects. In our view this result shows the necessity to check any dense surface alloy for electronic effects in order to avoid a misinterpretation of STM results.

ACKNOWLEDGMENTS

We would like to thank Professor J. Treusch and Professor H. Keiter for the support which made this work possible. Furthermore, we would like to thank Professor H. van Kempen for permission to include Fig. 5 in this paper. This work was supported by the DFG under Grants Nos. BL444/1-1 and WI1277/6-1, by the Program ''Verbundforschung Synchrotronstrahlung'' of the BMBF, and the TMR Networks, Contracts No. EMRX-CT96-0089 and FMRX-CT98-0178.

[1] T. Flores, M. Hansen, and M. Wuttig, Surf. Sci. **279**, 251 (1992).
[2] T. Flores, S. Junghans, and M. Wuttig, Surf. Sci. **371**, 1 (1997).
[3] T. Flores, S. Junghans, and M. Wuttig, Surf. Sci. **371**, 14 (1997).
[4] M. Wuttig, B. Feldmann, and T. Flores, Surf. Sci. **331-333**, 659 (1995).
[5] M. Wuttig, C. Knight, T. Flores, and Y. Gauthier, Surf. Sci. **292**, 189 (1993).
[6] O. Rader, W. Gudat, C. Carbone, E. Vescovo, S. Blügel, R. Kläages, W. Eberhardt, M. Wuttig, J. Redinger, and F. J. Himpsol, Phys. Rev. B **55**, 5404 (1997).
[7] O. Rader, E. Vescovo, M. Vescovo, M. Wuttig, D. D. Sarma, S. Blügel, F. J. Himpsel, A. Kimura, K. S. An, T. Mizokawa, A. Fujimori, and C. Carbone, Europhys. Lett. **39**, 429 (1997).
[8] W. L. O'Brien, J. Zhang, and B. P. Tonner, J. Phys.: Condens. Matter **5**, L515 (1993).
[9] W. L. O'Brien and B. P. Tonner, J. Appl. Phys. **76**, 6468 (1994).
[10] W. L. O'Brien and B. Tonner, Phys. Rev. B **51**, 617 (1995).
[11] D. Schmitz, O. Rader, C. Carbone, and W. Eberhardt, Phys. Rev. B **54**, 15 352 (1996).
[12] M. Wuttig, Y. Gauthier, and S. Blügel, Phys. Rev. Lett. **70**, 3619 (1993).
[13] C. Ross, B. Schirmer, M. Wuttig, Y. Gauthier, G. Bihlmayer, and S. Blügel, Phys. Rev. B **57**, 2607 (1998).
[14] B.-C. Choi, P. J. Bode, and J. Bland, Phys. Rev. B **58**, 5166 (1998).
[15] M. Wuttig, T. Flores, and C. Knight, Phys. Rev. B **48**, 12 082 (1993).
[16] D. Tian, R. F. Lin, and F. Jona, Solid State Commun. **74**, 1017 (1990).

[17] P. Schieffer, C. Krembel, M. C. Hanf, and G. Gewinner, Phys. Rev. B **55**, 13 884 (1997).
[18] P. Schieffer, C. Krembel, M. Hanf, and G. Gewinner, Phys. Rev. B **57**, 1141 (1998).
[19] W. Kim, S. J. Oh, J. Seo, J.-S. Kim, H.-G. Min, and S. C. Hong, Phys. Rev. B **57**, 8823 (1998).
[20] H. P. Noh, T. Hashizume, D. Jeon, Y. Kuk, H. W. Pickering, and T. Sakurai, Phys. Rev. B **50**, 2735 (1994).
[21] R. van der Kraan and H. van Kempen, Surf. Sci. **338**, 19 (1995).
[22] M. Wuttig, S. Junghans, T. Flores, and S. Blügel, Phys. Rev. B **53**, 7551 (1996).
[23] J. Tersoff and D. Hamann, Phys. Rev. Lett. **50**, 1998 (1983).
[24] M. Weinert, E. Wimmer, and A. J. Freeman, Phys. Rev. B **26**, 4571 (1982).
[25] E. Wimmer, H. Krakauer, M. Weinert, and A. Freeman, Phys. Rev. B **24**, 864 (1981).
[26] S. Vosko, L. Wilk, and N. Nusair, Can. J. Phys. **58**, 1200 (1980).
[27] S. Cunningham, Phys. Rev. B **10**, 4988 (1974).
[28] J. Tersoff, Phys. Rev. B **41**, 1235 (1990).
[29] J. A. Stroscio, D. T. Pierce, A. Davies, R. J. Celotta, and M. Weinert, Phys. Rev. Lett. **75**, 2960 (1995).
[30] S. Heinze, S. Blügel, R. Pascal, M. Bode, and R. Wiesendanger, Phys. Rev. B **58**, 16 432 (1998).
[31] W. A. Hofer, G. Ritz, W. Hebenstreit, M. Schmid, P. Varga, J. Redingor, and R. Podloucky, Surf. Sci. **405**, L514 (1998).
[32] S. Heinze, R. Abt, S. Blügel, G. Gilarowski, and H. Niehus, Phys. Rev. Lett. **83**, 4808 (1999).
[33] In this paper the vertical distance z is always measured between the center of the surface and tip atom (nucleus-nucleus distance).
[34] C. Chen, *Introduction to Scanning Tunneling Microscopy* (Oxford University Press, New York, 1993).
[35] T. Asada and S. Blügel, Physica B **237-238**, 359 (1997).
[36] A. Shick, A. I. Lichtenstein, and W. E. Pickett, Phys. Rev. B **60**, 10 763 (1999).
[37] G. Bihlmayer, R. Abt, S. Blügel, and T. Asada, in *International Symposium on Structure and Dynamics of Heterogeneous Systems*, edited by P. Entel (World Scientific, Singapore, 2000).